

# Production and Characterization of Pb-Carbon Composite for Manufacturing Metal Grids Applied in Lead-Acid Batteries

Caio Marcello Felbinger Azevedo Cossu<sup>a\*</sup> , Heverson Renan de Freitas<sup>c</sup>,

Monique Osório Talarico da Conceição<sup>b</sup>, Liana Alvares Rodrigues<sup>a</sup> ,

Marco Antonio Coelho Berton<sup>c</sup> , Carlos Angelo Nunes<sup>a</sup>

<sup>a</sup>Universidade de São Paulo, Escola de Engenharia de Lorena, Lorena, SP, Brasil.

<sup>b</sup>Universidade do Estado do Rio de Janeiro, Faculdade de Tecnologia, Resende, RJ, Brasil.

<sup>c</sup>Instituto SENAI de Inovação em Eletroquímica, Curitiba, PR, Brasil.

Received: January 02, 2024; Accepted: March 16, 2024

For decades, lead-acid batteries have been supplying power to electrical systems through redox reactions involving Pb and PbO<sub>2</sub>. However, the energy supply capacity is inherently constrained by low energy density and challenges associated with charge/discharge cycles. Studies have indicated that additions of C to the composition of the active mass improve the electrochemical properties of batteries. This work aims to produce, characterize the microstructure and evaluate the electrochemical properties of Pb-Carbon composites, comparing different types of C (graphite, graphene and xerogel). The samples were produced through powder metallurgy, pressed at 550 MPa and sintered at 320°C-48 h. The microstructure was characterized by XRD, SEM/EDS, and Vickers microhardness. Electrochemical analyses were evaluated through OCP, polarization, and cyclic voltammetry (CV) measurements in a solution of 4.91 mol·L<sup>-1</sup> of H<sub>2</sub>SO<sub>4</sub>. Microstructural characterizations revealed dispersions of C particles in the Pb matrix and an increase in the microhardness of the composites. Electrochemical analyses showed an increase in polarization resistance and a reduction in the corrosion rate compared to Pb. CV curves, demonstrated that C particles enhanced electrical conductivity for the formation of PbSO<sub>4</sub> and PbO<sub>2</sub>, allowing greater absorption of electrical overpotentials when compared to Pb, thereby improving charge/discharge cycles in positive grids.

**Keywords:** Powder Metallurgy, Pb Carbon Composites, Microstructural characterization, Electrochemical characterization.

## 1. Introduction

The new generation of electronic systems seeks the development of new energy storage systems. Lead-acid batteries have been a low-cost alternative for storing energy and promoting the functioning of electrical systems<sup>1</sup>.

The first batteries were of the SLI (Start, Lighting and Ignition) type, where, basically, energy is supplied only to the starting, lighting and ignition systems, restricting their use to other components. Currently, systems such as “start-stop” disable greater performance in charge/discharge processes, leading to the appearance of EFB (Enhanced Flooded Battery) type batteries and later VRLA (Valve Regulated Lead Acid) batteries<sup>2-6</sup>.

The energy provided by batteries involves spontaneous chemical oxidation-reduction reactions between the positive (PbO<sub>2</sub> → PbSO<sub>4</sub>) and negative (Pb → PbSO<sub>4</sub>) plates, forming PbSO<sub>4</sub> crystals on the surface of the positive and negative plates, providing ~ 2V to electrical circuits. This theory is known as the Double Sulfate Theory<sup>7</sup>.

The battery charging process occurs by inverting the direction of the discharge redox half-reactions. The inversion of the electrical current promotes the breakdown of the PbSO<sub>4(s)</sub> layer at the electrode/electrolyte interface to form Pb<sub>(s)</sub> and PbO<sub>2(s)</sub> on the surface of the grids. According to Kitoronka<sup>8</sup> the lead-acid batteries had a useful life of 1500 charge/discharge cycles, reaching 80% of discharge depth, with efficiency between cycles of 80% to 90%. According to Lam et al.<sup>9</sup>, the formation of PbSO<sub>4(s)</sub> crystals on the surface of the metal grids, acts as an electrical insulator, preventing the passage of electric current to reverse the direction of the redox reactions described above, impairing the charging process of the batteries. Bullock<sup>10</sup> stated that above 60°C, the solubility of the PbSO<sub>4(s)</sub> layer, after the discharge process, decreases drastically, increasing the concentration of H<sub>2</sub>SO<sub>4(aq)</sub>. The increase in the concentration of sulfuric acid, due to the diffusion of HSO<sub>4(aq)</sub><sup>-</sup> ions, displaces the reaction sites, creating an undesirable insulating barrier, limiting the charge reactions, decreasing the useful life, and consequently, battery loss.

\*e-mail: caio.cossu@usp.br

Yolshina et al.<sup>11</sup> presented a new proposal for the development of new grids using molten salts for the incorporation of carbon particles in the Pb matrix from  $\text{TiC}_{(s)}$ . The carbon inclusions form new crystalline phases that inhibit the growth of  $\text{PbSO}_{4(s)}$  crystals on the surface of the electrodes, improving the charging process of the batteries, increasing the capacitive effect of the metallic grids, reducing the evolution of  $\text{H}_{2(g)}$  (negative plate) and  $\text{O}_{2(g)}$  (positive plate) during the charging process. Yin et al.<sup>12</sup> highlighted that the carbon inclusions act as a toughener of the Pb matrix, increasing the mechanical resistance of the metallic grids.

This work aims to produce Pb-Carbon composites using the powder metallurgy route and evaluate the influence of different carbon particles in the Pb matrix on the charging and discharging processes and the morphology of the crystals formed after electrochemical tests.

## 2. Experimental Procedures

### 2.1. Processing

Pb powder (CNPC Powder® PB300, 99.9% purity) and graphene powder (2DM®, 99.9% purity), graphite (Nacional de Grafite®, 99.99% purity) and xerogel were used. (DEQUI/EEL-USP, 99.9%). The powder mixtures (~5 g) were homogenized manually by maceration for 2 min, producing mixtures containing 1 wt% graphite (Pb-1C<sub>graphite</sub>), 1 wt% graphene (Pb-1C<sub>graphene</sub>) and 1 wt% xerogel (Pb-1CX) and uniaxially compacted at 550 MPa producing bodies of test cylindrical samples with ~12 mm in diameter and ~4 mm in thickness. All samples were encapsulated under primary vacuum (~0,01 mbar) and sintered at 320°C for 48 h.

### 2.2. Characterization

The crystalline phases of the sintered samples were characterized by X-ray diffraction (XRD) in bulk form, previously sanded, in the Panalytical® Empyrean equipment operating with Cu-K $\alpha$  ( $\lambda = 1.5418 \text{ \AA}$ ) radiation from 20° to 80° and speed of 0.05°/s at room temperature. The crystalline phases were identified by comparing the diffractograms with the PDF4 database provided by the ICDD.

The morphology of the grains and the chemical composition of the samples were carried out by SEM/EDS using the Oxford® SwiftED3000 equipment coupled to the SEM Hitachi® TM3000. Due to the low hardness of the material, the samples were manually sanded with  $\text{Al}_2\text{O}_3$  sandpaper (P320, P400 and P600), and chemically polished in a 1:5 solution of glacial acetic acid and 30% hydrogen peroxide, for 60 s. The chemical composition of the samples was obtained by mapping three distinct regions for 300 s. The result of the chemical composition of the Pb-Carbon composites was based on the arithmetic mean of the chemical composition of these regions.

### 2.3 Electrochemical tests

The electrochemical tests were carried out on the Solartron® SI 1287 potentiostat with a three-electrode system: Reference Electrode (SCE), Counter-Electrode (Pt) and Working Electrode (Pb or Pb-Carbon). The exposure area for carrying out the electrochemical tests was

~1.13 cm<sup>2</sup> ( $\text{O}_D = 12 \text{ mm}$ ) in 4.91 mol•L<sup>-1</sup> solution of  $\text{H}_2\text{SO}_4$ , simulating the operating conditions of VRLA type lead-acid batteries at room temperature.

The samples were subjected to potentiostatic treatment, applying a cathodic potential of -0.5 V (vs SEC) until current stabilization ( $< \pm 200 \mu\text{A}\cdot\text{cm}^{-2}$ ) to remove the oxide layers on the surface of the electrodes.

Thermodynamic stability was verified by OCP measurements for 24 h. The identification of potentials for the formation of Pb,  $\text{PbSO}_4$ , PbO and  $\text{PbO}_2$  were obtained by applying the potentiodynamic polarization technique in 4.91 mol•L<sup>-1</sup> solution of  $\text{H}_2\text{SO}_4$ , between potentials from -1.2 to +2.0 V (vs SEC) at 10 mV•s<sup>-1</sup>. The electrochemical parameters ( $j_{\text{corr}}$ ,  $E_{\text{corr}}$ ,  $R_p$  and Corrosion Rate) were obtained using the Tafel straight line extrapolation method on potentiodynamic polarization curves (ASTM G3–89)<sup>13</sup> using Scribner® CView v.3.5 software.

The battery operation process was simulated, using the cyclic voltammetry technique to observe the formation of new layers on the surface of the grids during the charge/discharge processes of the positive and negative plates. In the positive grids, the sweep potential varied from +1.1 to +2.2 V (vs SEC) at 10 mV•s<sup>-1</sup> for 100 cycles.

## 3. Results and Discussions

### 3.1. Sample characterization

The low wettability and the large difference in specific mass between C (~2.27 g•cm<sup>-3</sup>) and Pb (~11.34 g•cm<sup>-3</sup>) made it unfeasible to produce samples using the casting route, segregating the carbon particles in liquid Pb during casting.

As an alternative route, the samples were produced using powder metallurgy, allowing the C particles to be dispersed in the Pb matrix for the production of Pb-Carbon composites.

All samples were sintered close to the melting temperature, due to the low sinterability of Pb. After sintering at 320°C for 48 h, the samples produced showed a relative density greater than 93%.

The results by X-ray diffractometry (XRD), presented in Figure 1, identified the peaks of carbon particle (~55°) in Pb matrix. Other peaks were identified (PbO) related to the reactivity between Pb and residual  $\text{O}_2$  during the sintering process at 320°C for 48 h, forming PbO on the surface of the samples<sup>14</sup>.

SEM analyzes showed three distinct phases on the surface of the samples after sintering, due to the color contrast, characteristic of the chemical composition of the phases. It was observed that chemical polishing promoted oxidation ( $\text{Pb} \rightarrow \text{PbO}$ ) in the intergranular region, revealing the morphology of the Pb grains and the distribution of carbon particles in this region. Table 1 shows the chemical composition of the surface of the composites, quantifying the presence of carbon particles in the Pb matrix, corroborating the XRD results and identified by SEM.

Yin et al.<sup>12</sup> mentioned that dispersions of particles with higher hardness than the matrix increase the mechanical resistance of these alloys. Table 2 compares the Vickers microhardness of Pb, the Pb Carbon composites produced in this article and the alloys produced by other authors.

Luip, C.; Pilone, D<sup>15</sup>. observed the influence of Sb addition on the microhardness and electrochemical behavior of Pb-Ag

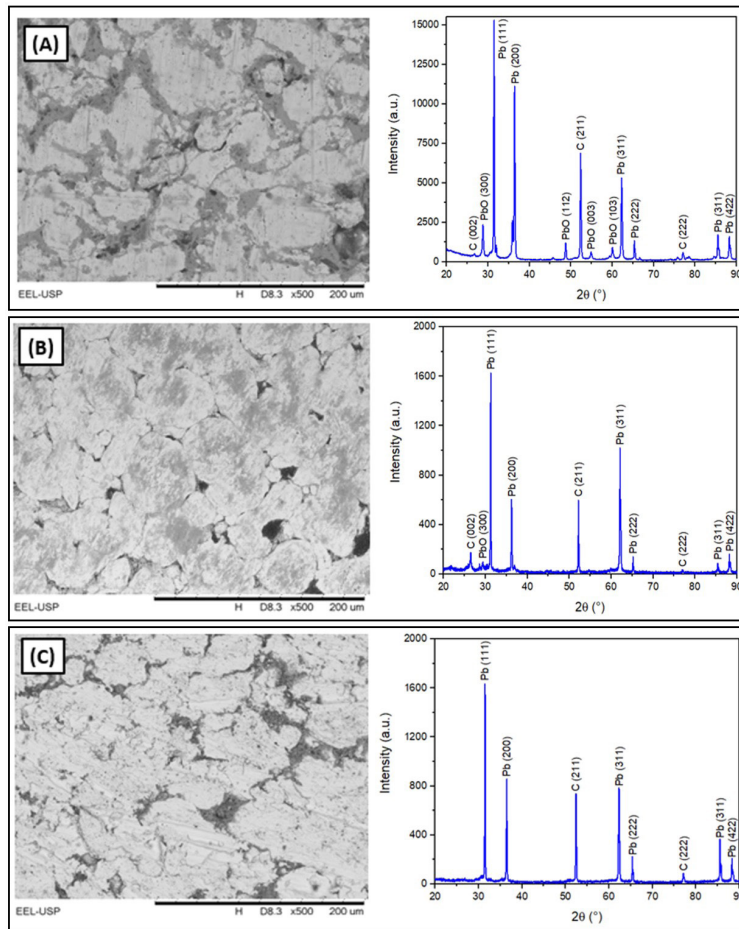


**Figure 1.** XRD and SEM of composites Pb-Carbon: (a) Pb-1C<sub>graphene</sub>, (b) Pb-1C<sub>graphite</sub> and (c) Pb-1CX sintered under primary vacuum at 320°C for 48 h.

**Table 1.** EDS analysis using the mapping technique for 300 s on the composites Pb-1C<sub>graphite</sub>, Pb-1C<sub>graphene</sub> and Pb-1CX sintered under primary vacuum at 320°C for 48 h.

Samples	Element		
	Carbon	Lead	Oxygen
Pb-1C <sub>graphite</sub>	7.193 ± 0.53 wt.%	68.365 ± 1.18 wt.%	24.442 ± 0.16 wt.%
Pb-1C <sub>graphene</sub>	7.187 ± 0.37 wt.%	68.384 ± 2.47 wt.%	24.428 ± 0.95 wt.%
Pb-1CX	6.386 ± 0.81 wt.%	71.109 ± 1.81 wt.%	22.505 ± 1.52 wt.%

and Pb-Ag-Sb system alloys. The addition of Sb promoted an increase in microhardness where the Pb-0.2%Ag-0.2%Sb alloy (6.3 HV) showed better results. El-Sayed et al.<sup>16</sup> studied the effect of additions of Sb, Zn, Cu and Ag in Pb-5%Sn binary alloys (wt.%) produced by “melt-spinning” and cold rolled. The cold-rolled Pb-5%Sn-0.5%Cu alloy (8.8 HV) showed the best results.

In comparison, the Vickers microhardness of the Pb-Carbon composites presented higher values than the Pb sample (9.3 HV), varying between 10.4 HV (Pb-1CX) and 14.1 HV (Pb-1C<sub>graphene</sub>), showing that the carbon particles promote an increase in the mechanical resistance of the alloys.

### 3.2 Electrochemical tests

It was observed that the dispersion of carbon particles promotes the stabilization of the electrode at more positive potentials when compared to the Pb sample after 5 h of exposure in H<sub>2</sub>SO<sub>4</sub> solution in open circuit (OC). According Wolynec<sup>17</sup> these measurements reveal two steps to identify the thermodynamic stability potential of the electrodes:

- (i) metallic dissolution at the electrode/electrolyte interface (Pb → Pb<sup>2+</sup>) until reaching the saturation limit of the solution in the electrical double layer with Pb<sup>2+</sup> ions;
- (ii) the consumption of Pb<sup>2+</sup> ions leads to the formation of the PbSO<sub>4</sub> passivating film on the electrode surface.

**Table 2.** Comparison of Vickers microhardness values of samples produced from Pb and Pb-Carbon composites and alloys produced by other authors.

Composition (wt.%)	Microhardness	Manufacturing process	Reference
Pb-0.8Ag	5.8	As cast	Lupi and Pilone <sup>15</sup>
Pb-0.05Ca	9.3		
Pb-5Sn	6.5	Melt-spinning	El-Sayed et al. <sup>16</sup>
Pb-5Sn-0.5Sb	6.2		
Pb-5Sn-0.5Ag	7.8	Cold rolled	This work
Pb-5Sn-0.5Sb	8.7		
Pb-5Sn-0.5Cu	8.8		
Pb	<b>9.3 ± 0.2</b>	<b>Uniaxial pressed at 550 MPa and sintered at 320°C-48 h</b>	<b>This work</b>
Pb-1C <sub>graphite</sub>	<b>13.0 ± 0.6</b>		
Pb-1C <sub>graphene</sub>	<b>14.1 ± 0.4</b>		
Pb-1CX	<b>10.7 ± 0.5</b>		

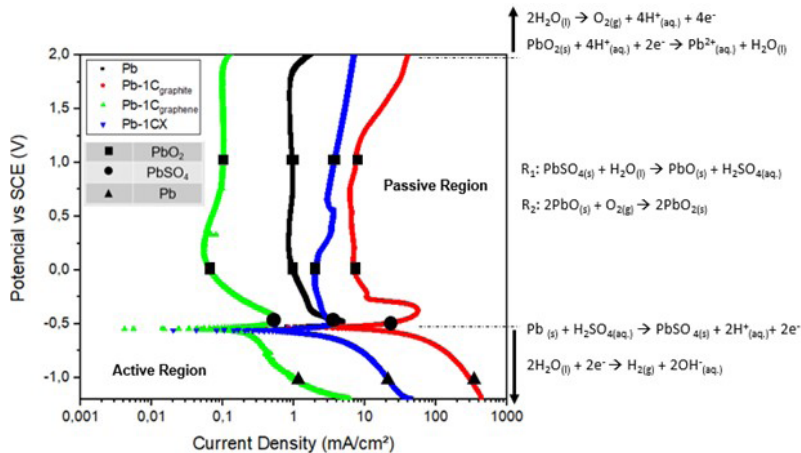


**Figure 2.** Potentiodynamic polarization curves of Pb and the composites P-1C<sub>graphite</sub>, Pb-1C<sub>graphene</sub> and Pb-1CX sintered at 320°C for 48 h in 4.91 mol·L<sup>-1</sup> H<sub>2</sub>SO<sub>4</sub> solution.

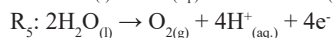
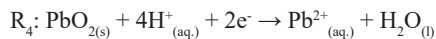
The stabilization at more positive potentials of Pb-Carbon composites when compared to Pb suggests that these composites are more noble, but not conclusive, using this technique alone<sup>18,19</sup>

Figure 2 compares the potentiodynamic polarization curves of the Pb and Pb-Carbon composites. The analysis of polarization curves allowed the identification of the active, passive and transpassive regions for the formation of films (Pb, PbSO<sub>4</sub>, PbO/ PbO<sub>2</sub>) on the surface of the samples.

It was observed that the dispersion of carbon particles did not promote the displacement of the corrosion potential in +0.53 V (vs SCE) for the formation of the PbSO<sub>4</sub> layer (reaction R<sub>1</sub>) on the surface of the Pb-Carbon composites. In the analyzed samples, the formation potentials of the PbO/PbO<sub>2</sub> layer (reaction R<sub>2</sub> and R<sub>3</sub>) were close to +0.25 V (vs SCE). The passivation region varied between +0.25 and +2.0 V (vs SCE) in all samples. This result allowed us to conclude that the inclusion of carbon particles in the Pb matrix does not displace the electrical potentials for the formation

of passivating oxides. It was observed that carbon particles improve the polarization resistance of the composites, causing a decrease in the corrosion rate of the composites due to the decrease in the corrosion current density ( $j_{\text{corr}}$ ), as shown in the results in Table 3, obtained by the methods of extrapolation of the Tafel straight line in potentiodynamic polarization curves.

Above 2.0 V (vs SEC), the transpassivation region begins, promoting the disruption of the passivating layers (PbO/PbO<sub>2</sub>), releasing Pb<sup>2+</sup> ions into the solution (R<sub>4</sub>), accelerating the process of O<sub>2</sub> evolution in the positive plates (R<sub>5</sub>).



D'Alkaine et al.<sup>20</sup>, mentions that the evolution of O<sub>2</sub> is undesirable, as the increase in the pH of the electrolyte displaces the reaction sites for the formation of PbSO<sub>4</sub> during the discharge process, causing sulfation of the positive plates.

Yolshina et al.<sup>11</sup> mentions that the addition of carbon particles increases the capacitive effect of Pb-Carbon composites, reducing the O<sub>2</sub> evolution process.

### 3.3. Cyclic voltammetry

Figure 3 shows the cyclic voltammetry curves of the Pb-Carbon composites and the SEM after 100 charge/discharge cycles.

SEM analyzes showed that corrosion of the grids during charge/discharge cycles occurred in the intergranular region. The dispersions of carbon particles promoted an increase in electrical conductivity, intensifying the electric field for the formation of PbSO<sub>4</sub> and PbO<sub>2</sub> layers and limiting the bidirectional growth of these layers.

In the discharge direction ( $i_{p,c}$ ), the formation peak of PbSO<sub>4</sub> layer (PbO<sub>2</sub> → PbSO<sub>4</sub>) was observed on the surface of

**Table 3.** Parameter results applying the Tafel straight line extrapolation method in the potentiodynamic polarization curves and open circuit potential after 5 h of exposure in a solution of 4.91 mol·L<sup>-1</sup> H<sub>2</sub>SO<sub>4</sub>.

Samples	E <sub>OCP</sub> [V] (vs SCE)	j <sub>corr.</sub> [mA/cm <sup>2</sup> ]	E <sub>corr.</sub> [V] (vs SCE)	R <sub>p</sub> [Ω]	Corrosion rate [mm·y <sup>-1</sup> ]
Pb	-0.208	32.25	-0.52	8.33	217.97
Pb-1C <sub>graphite</sub>	-0.198	12.04	-0.53	24.99	85.13
Pb-1C <sub>graphene</sub>	-0.152	0.192	-0.54	182.93	13.79
Pb-1CX	-0.194	1.325	-0.55	25.69	103.57

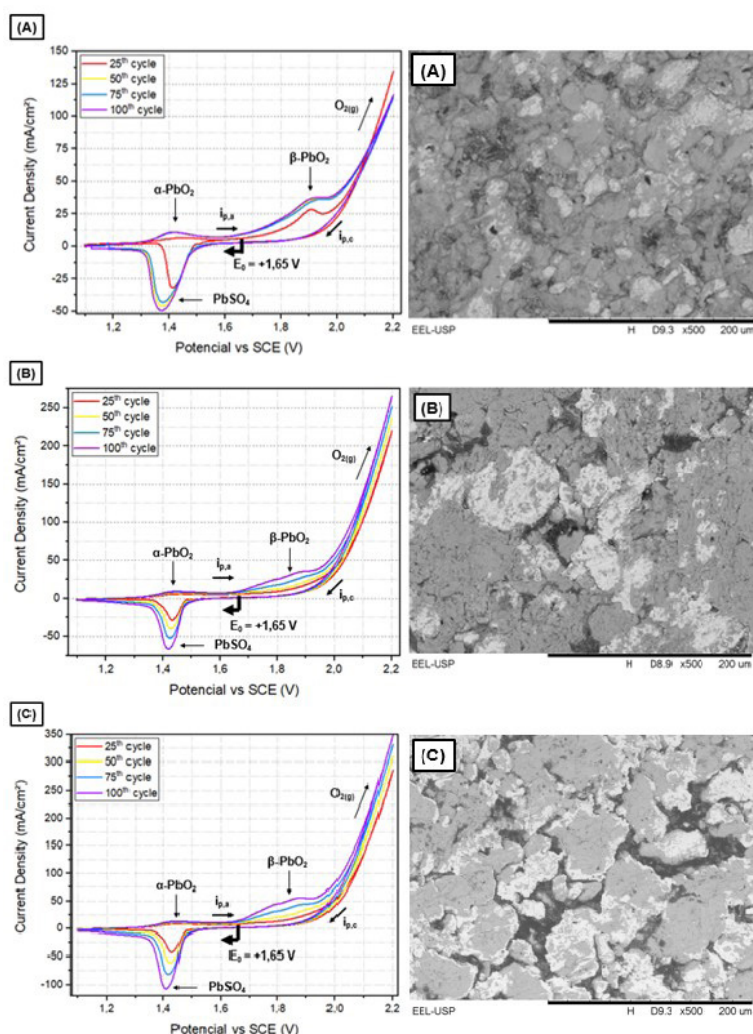


**Figure 3.** Cyclic voltammetry curves and SEM of the Pb-Carbon composites after 100 cycles in a 4.91 mol·L<sup>-1</sup> H<sub>2</sub>SO<sub>4</sub> solution: (a) Pb-1C<sub>graphite</sub>; (b) Pb-1CX and (c) Pb-1C<sub>graphene</sub>.

**Table 4.** Comparison of current density in anodic/cathodic peaks and determination of the diffusion coefficient for the formation of PbSO<sub>4</sub> and PbO<sub>2</sub> layers applying the Nernst equation comparing the Pb and Pb-Carbon sample.

Samples	$i_{a,p}$ [mA·cm <sup>-2</sup> ]	$i_{c,p}$ [mA·cm <sup>-2</sup> ]	$D_{0(i_{a,p})}$ [10 <sup>-21</sup> cm <sup>2</sup> ·s <sup>-1</sup> ]	$D_{0(i_{c,p})}$ [10 <sup>-21</sup> cm <sup>2</sup> ·s <sup>-1</sup> ]
Pb	25.90	46.31	3.76	12.03
Pb-1C <sub>graphite</sub>	33.33	66.15	6.23	24.56
Pb-1C <sub>graphene</sub>	56.00	106.91	17.60	64.14
Pb-1CX	38.72	73.44	8.41	30.27

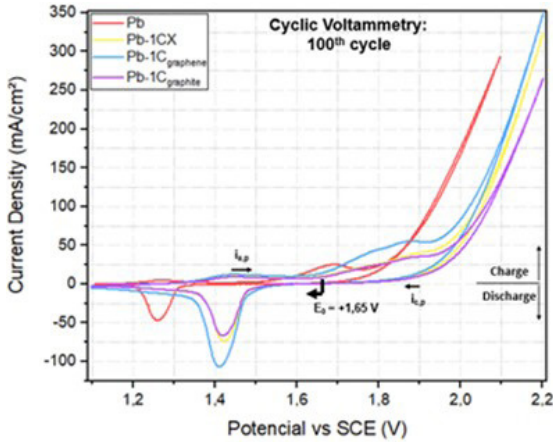


**Figure 4.** Comparison of the cyclic voltammetry curves of Pb and Pb-Carbon composites after 100 cycles in a solution of 4.91 mol·L<sup>-1</sup> H<sub>2</sub>SO<sub>4</sub> between potentials of +1.1 and +2.2 V (vs SCE) at 10 mV·s<sup>-1</sup>.

the grids at +1.4 V (vs SCE). By reversing the direction ( $i_{p,a}$ ), two anodic peaks were identified. The first peak, at +1.4 V (vs SCE), comes from the oxidation of PbSO<sub>4</sub> →  $\alpha$ -PbO<sub>2</sub>, and the second peak, at +1.9 V (vs SCE), from the formation of the  $\beta$ -PbO<sub>2</sub> phase on the surface of the samples. At higher potentials, the increase in current density characterizes the disruption of the layer of passivating oxides, initiating the O<sub>2</sub> evolution process, with a return at +2.2 V (vs SCE), corroborating the results obtained by Fletcher<sup>21</sup>.

The CV curves of the Pb-Carbon composites also revealed that the formation peaks of the PbSO<sub>4</sub> and  $\alpha$ -PbO<sub>2</sub> layers occur at the same potential, at +1.4 V (vs SCE), suggesting that the charge/discharge process is reversible.

In reversible or almost reversible processes, the Nernst equation (Equation 2) makes it possible to associate the anodic/cathodic current peaks with the diffusion coefficient for the formation of PbSO<sub>4</sub> and  $\alpha$ -PbO<sub>2</sub> layers, as shown in the Table 4.

$$i_p = \left(2,69 \cdot 10^8\right) \cdot n^{3/2} \cdot A \cdot C \cdot D_0^{1/2} \cdot v^{1/2} \quad \text{Eq. 2}$$

where:  $i_p$  = peak current [A·cm<sup>-2</sup>];  $n$  = number of electrons in the reaction ( $n = 2 e^-$ );  $A$  = surface area (~1.13 cm<sup>2</sup>);  $C$  = electrolyte concentration (~4.91 mol·L<sup>-1</sup>);  $D_0$  = diffusion coefficient [cm<sup>2</sup>·s<sup>-1</sup>];  $v$  = scan rate (0.010 V·s<sup>-1</sup>).

Figure 4 compares the cyclic voltammetry curves of Pb and Pb-Carbon composites after the cyclic voltammetry in

a solution of 4.91 mol·L<sup>-1</sup> H<sub>2</sub>SO<sub>4</sub> for 100 cycles between potentials of +1.1 and 2.2 V (vs SCE) by 10 mV·s<sup>-1</sup>.

The cyclic voltammetry curves (Figure 4) and the results presented in Table 4 indicated that the C particles promoted an increase in the diffusion of SO<sub>4</sub><sup>2-</sup> ions in the adsorption/desorption processes for the formation of PbSO<sub>4</sub> layers (discharge process) and PbO<sub>2</sub> layers (charge process), as evidenced by the enhancement of anodic/cathodic peaks. This suggests that the C particles enhance the reaction rate for the formation of new layers on the electrode surfaces.

The electric potentials for the formation of PbSO<sub>4</sub> and PbO<sub>2</sub> peaks in the Pb-Carbon composites shifted to the right (~0.2 V vs SCE), improving the electrochemical properties with a decrease in O<sub>2</sub> evolution at higher overpotentials. The area under the CV curves ( $j_{corr}$  vs. potential) showed that the Pb-Carbon composites exhibited enhanced electrical charge transport, and consequently, the electrical conductivity of the composite yielded superior results compared to pure Pb, corroborating the results of other authors<sup>11,22,23</sup>.

## 4. Conclusion

In the quest for alternative pathways in developing new materials for manufacturing metal grids in lead-acid batteries, the powder metallurgy approach demonstrated remarkable effectiveness in producing advanced Pb-Carbon composites.

The dispersion of C particles in the Pb matrix was identified, significantly enhancing both the mechanical and electrochemical properties of the composites compared to pure Pb. In contrast to various Pb alloys reported by several authors, Pb-Carbon composites exhibited an approximately 10% higher Vickers hardness.

Electrochemical analyses revealed a constant corrosion potential ( $E_{corr}$ ) at -0.53 V (vs SCE) and a lower corrosion rate in Pb-Carbon composites compared to pure Pb, indicating the role of carbon particles in increasing the polarization resistance ( $R_p$ ) of the grids.

Notably, the CV curves, after 100 cycles, showed a deviation of +0.2 V (vs SCE). This shift proved crucial in enhancing the composites' ability to absorb electrical overpotentials, effectively mitigating high rates of O<sub>2</sub> evolution and increasing the amplitude of anodic and cathodic peaks, owing to the improved electrical conductivity and higher electrochemical efficiency in forming PbSO<sub>4</sub> and PbO<sub>2</sub> layers on the sample surfaces.

Comparing the different C particles, all samples exhibited similar behavior, with the sample containing graphene carbon particles standing out, demonstrating superior results compared to graphite carbon and xerogel. However, the

high cost associated with graphene particles may warrant consideration for their substitution with other carbon variants offering a more favorable cost-benefit ratio in Pb-Carbon composite production.

## 5. Acknowledgments

The authors acknowledge the CNPq for financial support.

## 6. Reference

1. Anderman M. The challenge to fulfill electrical power requirements of advanced vehicles. *J Power Sources*. 2004;127(1-2):2-7. <http://doi.org/10.1016/j.jpowsour.2003.09.002>.
2. Bagshaw NE. Battery grid alloys: principles and practice. *J Power Sources*. 1989;12:113-29.
3. Moseley PT. Consequences of including carbon in the negative plates of Valve-regulated Lead-Acid batteries exposed to high-rate partial-state-of-charge operation. *J Power Sources*. 2009;191(1):134-8. <http://doi.org/10.1016/j.jpowsour.2008.08.084>.
4. Berndt D. Valve regulated lead-acid batteries. *J Power Sources*. 2001;100(1-2):29-46. [http://doi.org/10.1016/S0378-7753\(01\)00881-3](http://doi.org/10.1016/S0378-7753(01)00881-3).
5. Sanhueza AEC. Desenvolvidos na indústria de acumulação de energia de baterias chumbo-ácido: processos alternativos de recuperação de chumbo [thesis]. Bauru, São Paulo: Universidade Estadual Paulista; 2007. 144 p.
6. Bode H. Lead-acid batteries. New York: John Wiley & Sons; 1997. 387 p.
7. Singh PK. Energy storage systems for electric vehicles. In: ECN's Flipped Symposium; 2010; United Kingdom . Proceedings. UK: ATM; 2020. 6 p.
8. Kitoronka S. Lead-acid battery. India: Institute of Sciences, Electrical and Electronics; 2022.
9. Lam LT, Haigh NP, Phyland CG, Urban AJ. Failure mode of valve-regulated lead-acid batteries under high-rate partial-state-of-charge operation. *J Power Sources*. 2004;133(1):126-34. <http://doi.org/10.1016/j.jpowsour.2003.11.048>.
10. Bullock KR. Lead-acid battery research and development: a vital key to winning new business. *J Power Sources*. 2003;116(1-2):8-13. [http://doi.org/10.1016/S0378-7753\(02\)00700-0](http://doi.org/10.1016/S0378-7753(02)00700-0).
11. Yolshina LA, Yolshina VA, Yolshin AN, Plaksin SV. Novel lead-graphene and lead-graphite metallic composite materials for possible application as positive electrode grid in lead-acid battery. *J Power Sources*. 2015;278:87-97. <http://doi.org/10.1016/j.jpowsour.2014.12.036>.
12. Yin J, Lin N, Zhang W, Lin Z, Zhang Z, Wang Y, et al. Highly reversible lead-carbon battery anode with lead grafting on the carbon surface. *J Energy Chem*. 2018;27(6):1674-83. <http://doi.org/10.1016/j.jechem.2018.03.002>.
13. ASTM: American Society for Testing and Materials. ASTM G3-89: standard practice for conventions applicable to electrochemical measurements in corrosion testing. West Conshohocken: ASTM International; 1999. 10 p.
14. Inguanta R, Vergottini F, Ferrara G, Piazza S, Sunseri C. Effect of temperature on the growth of  $\alpha$ -PbO<sub>2</sub> nanostructures. *Electrochim Acta*. 2010;55(28):8556-62. <http://doi.org/10.1016/j.electacta.2010.07.073>.
15. Lupi C, Pilone D. New lead alloy anodes and organic depolariser utilization in zinc electrowinning. *Hydrometallurgy*. 1997;44(3):347-58. [http://doi.org/10.1016/S0304-386X\(96\)00060-6](http://doi.org/10.1016/S0304-386X(96)00060-6).
16. El-Sayed MM, Abd El-Salam F, Nada RH, Kamal M. Effect of ternary addition on characteristics of Pb-Sn base alloys. *J Solution Chem*. 2001;24(2):161-70.
17. Wolyneć S. Técnicas eletroquímicas em corrosão. São Paulo: Universidade de São Paulo; 2003. 166 p.
18. Cheng Y, Wilmott M, Luo J. Analysis of the role of electrode capacitance on the initiation of pits for A516 carbon steel by electrochemical noise measurements. *Corros Sci*. 1999;41(7):1245-56. [http://doi.org/10.1016/S0010-938X\(98\)00181-4](http://doi.org/10.1016/S0010-938X(98)00181-4).
19. Arya SB, Joseph FJ. Electrochemical methods in tribocorrosion. In: Siddaiah A, Ramachandran R, Menezes P, editors. Tribocorrosion: fundamentals, methods and materials. London: Academic Press; 2021. Chapter 3; p. 43-77. <http://doi.org/10.1016/B978-0-12-818916-0.00003-1>.
20. D'Alkaine CV, Garcia CM, Brito GAO, Pratta PMP, Fernandes FP. Disruption processes in films grown and reduced electrochemically on metals. *J Solid State Electrochem*. 2007;11:1575-83. <http://doi.org/10.1007/s10008-007-0361-x>.
21. Fletcher S. Some recent developments in electrochemical nucleation-growth-collision theory. *J Electroanal Chem Interfacial Electrochem*. 1981;118:419-32. [http://doi.org/10.1016/S0022-0728\(81\)80558-X](http://doi.org/10.1016/S0022-0728(81)80558-X).
22. Liu HT, Yang CX, Liang HH, Yang J, Zhou WF. The mechanisms for the growth of the anodic Pb(II) oxides films formed on Pb-Sb and Pb-Sn alloys in sulfuric acid solution. *J Power Sources*. 2002;103(2):173-9. [http://doi.org/10.1016/S0378-7753\(01\)00839-4](http://doi.org/10.1016/S0378-7753(01)00839-4).
23. Takehara ZI. Dissolution and precipitation reactions of lead sulfate in positive and negative electrodes in lead acid battery. *J Power Sources*. 2000;85(1):29-37. [http://doi.org/10.1016/S0378-7753\(99\)00378-X](http://doi.org/10.1016/S0378-7753(99)00378-X).